Turkish Journal of Electrical Engineering & Computer Sciences

http://journals.tubitak.gov.tr/elektrik/

Research Article

Turk J Elec Eng & Comp Sci
(2018) 26: 1153 – 1163

doi:10.3906/elk-1710-118

Modeling of realistic heart electrical excitation based on DTI scans and modified reaction diffusion equation

Ihab ELAFF*
Department of Computer Engineering, Faculty of Engineering and Natural Sciences, Üsküdar University, İstanbul, Turkey

Received: 11.10.2017 • **Accepted/Published Online:** 24.01.2018 • **Final Version:** 30.05.2018

Abstract: A new method is proposed for modeling realistic heart activation using diffusion tensor imaging (DTI) scans based on biological properties of its tissues in addition to the working methodology of the DTI scanner. Modeling of the excitation propagation inside the heart is initiated by applying activation at only one pacing site at the root of the conduction network. The excitation propagation has been accomplished based on a proposed conduction system that is extracted from DTI heart scans and a modified version of monodomain reaction diffusion equation (RDE) that considers the heart inhomogeneous–anisotropic material. The Aliev–Panfilov method was used to model the reaction part of the equation and inhomogeneous–anisotropic diffusion to model the diffusion part in the equation. Variation in conduction speeds between the myocardium and the conduction system has been also taken into consideration. Employing the proposed conduction system and the modified RDE on the heart model shows (somewhat) realistic heart activation where the produced ventricular excitation propagation isochrones are similar to real measurements.

Key words: Reaction diffusion equation, heart, activation, excitation propagation, conduction system, Purkinje, diffusion tensor imaging

1. Introduction

The heart is the control unit of the circularity system, responsible for circulating blood throughout the body. Inefficient blood flow through the circularity system can cause inefficiency, damage, or malfunction of any of the body organs, including the heart itself [1]. Among different diseases, heart diseases are considered to be one of the major causes of death all over the world [1]. Cardiac arrhythmias are the most dangerous category of heart diseases and can lead to death within minutes if left untreated. Cardiac arrhythmias are any group of conditions that cause the electrical activity of the heart to be more irregular than normal [1,2]. Arrhythmia drugs are not always the best choice for managing patients, as sudden cardiac death may occur even with the correct dosage of the medicine [1].

The heart is located in the middle of the thorax and it is connected to the great vessels of the circularity system [2–6]. It consists of four compartments (chambers): the right atrium (RA), the left atrium (LA), the right ventricle (RV), and the left ventricle (LV). The outer wall of the heart is called the epicardium and the inner wall of the heart is called the endocardium. The muscle of the heart is called the myocardium. Each of the heart's chambers is connected to some of the circularity system vessels and the blood flow from atriums to ventricles is regulated by intermediate valves. The heart contains a special conduction system that is responsible

*Correspondence: ihab_el_aff@hotmail.com

for triggering its activity. The conduction system is started by special type of cell located on the wall of the RA that is called the sinoatrial (SA) node or the sinus node. The SA node is connected to special electrical conduction system that is responsible for activating the RA and the LA. The conduction system is extended to another node between atriums and ventricles (near the RA) called the atrioventricle (AV) node. The AV node is connected to the His bundle (common bundle) which is located in the interventricular septum (IV septum). The His bundle has two branches, a left branch to the LV and a right branch to the RV. These branches spread and form a network that covers ventricle walls [2–6]. This work is focused on activation of ventricles of the heart, as they represent the most powerful part of the heart since they occupy most of the heart's mass and are responsible for pumping blood towards organs, and inefficiency in their operation will be reflected in whole body organs as well as the heart itself. It is necessary to design a model that is capable of visualizing the electrical activities of the heart in 3D. Generating such visualizations can help cardiologists identify if the electrical propagation flows in an appropriate manner or not, and according to that they can propose suitable treatments.

2. Materials and methods

2.1. Data acquisition

The dataset used in this research is from a diffusion tensor imaging (DTI) scan of a male subject with no cardiac disease history and was downloaded from the Johns Hopkins University website. Data were stored in 3D matrices as a MATLAB file of size $256 \times 256 \times 134$ sample points (corresponding to $0.4297 \times 0.4297 \times 1.0$ mm), where each vortex in the matrix consists of three eigenvectors of diffusion, which represent the local fiber direction and cross-fiber directions, as well as three eigenvalues of diffusion in the direction of each eigenvector.

2.2. Heart tissue decomposition

Heart tissue can be classified into 2 main types: myocardium and conduction system. To simulate heart electrical activation, both structures must be identified, especially the conduction system, as it initiates the activation. The most common reference models used to identify the ventricular conduction system of the heart are those described by Tawara [7], Massing et al. [8], and Durrer et al. [9]. Modeling of the ventricular conduction systems involves either assigning the early activation sites according to the measurements of Durrer et al. [10–13] or building a network according to the heart anatomical structure and activation isochrones [14–17]. The conduction system of the ventricles varies considerably from heart to heart [8], which makes identifying the correct structure of the conduction system model subject to trial and error, as a small variation in conduction sites will produce a large variation in activation results. Other groups of models do not model any conduction system, as they use experimental pacing sites in their models [18–20].

By taking a close look at the conduction system, it would be possible to separate the real conduction system from DTI scans [21]. The conduction system contains a large number of modified cardiac cells, which are called Purkinje cells [22], and it also contains normal cardiac cells in its tracts [23,24]. Purkinje cells are different than these normal cardiac cells in several aspects, but the most important properties are that they have a smaller number of myofilaments and more glycogen than myocardium cells [22,23], which means Purkinje cells contain more water content than myocardium. Purkinje cells are connected to each other through highly developed interlaced disks, which are adapted for high conductivity of electrical current [23].

An MRI scanner is capable of showing low intensity areas for zones that contain low amounts of water and vice versa [25–28], which make the intensity level directly proportional to the amount of water in the

sample. Based on this fact, Purkinje tissues should appear with higher intensity than myocardium tissues. The DTI modality will provide the full information about the samples in 3D, while scalar indexes of the DTI will provide rotational invariant quantities that can be used to differentiate between different tissues. Among different scalar indexes, the diffusion volume (DV) quantity [21] is used to differentiate between different heart tissues because it can produce a high contrast mapping of different tissues. Low-intensity zones represent fatty tissue, medium-intensity zones represent myocardium tissue, and high-intensity zones represent Purkinje tissue (Figure 1). The produced DV map can be segmented with any clustering algorithm [29], such as K-means, and extra details are removed manually (Figure 2).

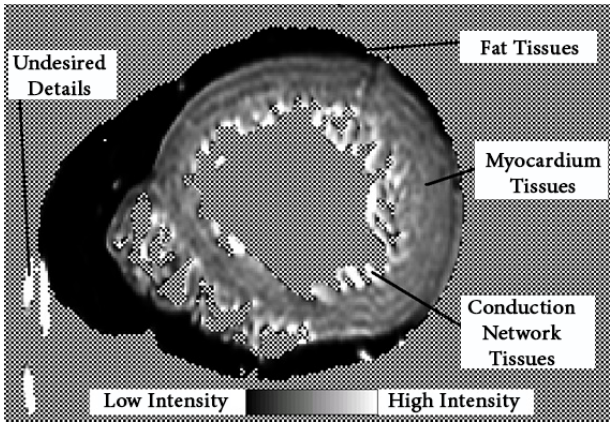

Figure 1. The DV intensity map for a heart slice (lighter zones correspond to more water content in the tissue and vice versa).

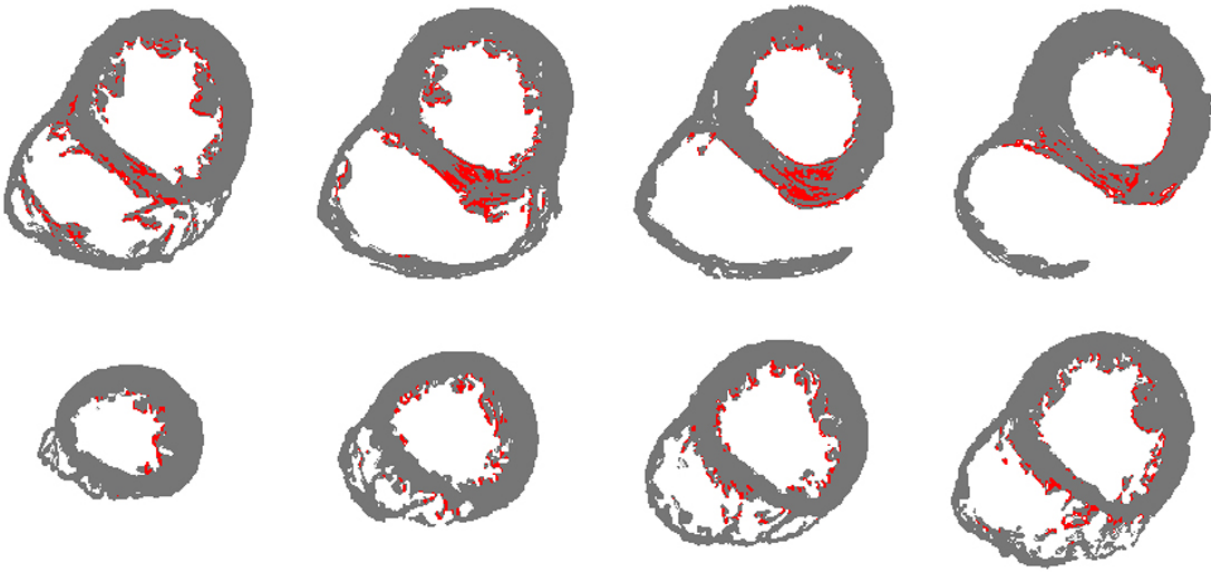

Figure 2. Segmentation of DV map using K-means. (Red regions represent Purkinje tissue and gray regions represent myocardium tissue.)

2.3. Modeling of the heart bioelectricity by reaction diffusion equation (RDE)

Modeling the bioelectricity of biological tissues has been introduced in many studies and verified to give acceptable results when compared with physical measurements. From physical measurements, Geselowitz [30] found that the following quasistatic conditions are applicable for biological tissues:

1. The biological tissues respond linearly to the electrical quantities.
2. The capacitance components of the body tissues can be neglected as the frequency of the electrical signal is low.
3. The signal rise time is very small (microseconds), which makes the time derivatives negligible.
4. The electromagnetic wave effect can be neglected.

Bioelectricity has its origins in the potential differences present between the intercellular space and the extracellular space for each cell, and so is called the bidomain. These potential differences produce current sources that generate electric potentials on the body surface (such as electrocardiograph) and magnetic fields outside the body (such as magnetocardiograph) [31].

The excitation propagation of bioelectricity inside excitable tissues like the heart and brain can be described by the bidomain RDE or the monodomain RDE. Modeling of the monodomain equation for excitation propagation has been introduced in different studies. However, using bidomain models requires more parameters and more computation time compared to monodomain models and differences between their results were extremely small [32]. The monodomain RDE, where all equation parameters will be in terms of the intercellular domain, would be as follows:

$$\frac{\partial V_m}{\partial t} = \frac{1}{C_m}\frac{1}{A_m}\frac{k}{1+k}\left[\nabla.(\sigma_i \nabla V_m)\right] - \frac{1}{C_m}\left[\Sigma I_{ions} + I_{app}\right], \tag{1}$$

where V_m is the transmembrance potential, C_m is the membrane capacitance, A_m is the surface-to-volume ratio of the membrane, k is the ratio between the extracellular and the intercellular conductivities, σ_i is the intercellular conductivity tensor, I_{ions} are ionic currents that cross the cell membrane during the reaction, and I_{app} is an external applied current that stimulates the cell membrane. Eq. (1) contains the diffusion term $\frac{1}{C_m}\frac{1}{A_m}\frac{k}{1+k}\left[\nabla.(\sigma_i \nabla V_m)\right]$ and the reaction term $\frac{1}{C_m}\left[\Sigma I_{ions} + I_{app}\right]$. As eigenvectors of diffusion are orthogonal and traverse conductivities are almost equal, the conductivity tensor σ_i is symmetric and positive definite, and it can be written as

$$\sigma_i = \sigma_{it} I + (\sigma_{il} - \sigma_{it}) e e^T, \tag{2}$$

where e represents the first eigenvector of the diffusion tensor, and σ_{il} and σ_{it} represent the intercellular conductivities in longitudinal and traverse directions, respectively, and I is the identity matrix, which yields

$$D = \frac{\sigma_{it}}{\sigma_{il}} I + (1 - \frac{\sigma_{it}}{\sigma_{il}}) e e^T = e \begin{bmatrix} 1 & 0 & 0 \\ 0 & \sigma_{it}/\sigma_{il} & 0 \\ 0 & 0 & \sigma_{it}/\sigma_{il} \end{bmatrix} e^T, \tag{3}$$

where D is the normalized effective conductivity tensor of the heart material. By substitution with appropriate values for C_m, A_m, k, σ_{it}, and σ_{il}, and normalizing V_m and t, the normalized form of monodomain RDE

can be written as

$$\frac{\partial u}{\partial t} = \nabla.(D\nabla u) + f + g, \tag{4}$$

where u and t represent the normalized transmembrance potential and the normalized time, respectively, f is the function that represents the reaction term due to ion exchange, and finally g represents the external applied input.

2.4. Electrical excitation methods of heart tissue

Modeling of the heart's electrical excitation (reaction part of the monodomain RDE) is presented on either the cellular scale [14,18,19] or for the whole tissue [10,11,15,33,34]. Some qualitative models have also been developed [20,35] to model cardiac excitation. The cellular scale models describe the cell action potential according to an individual cell. Cellular scale relates the effect of different ions' current to the variation in the action potential. The most famous model of this type of excitation model was introduced by Hodgkin and Huxley [36]. It is considered the first quantitative model that describes the excitation of the nerve cell. Many other quantitative models that represent the action potential in the cell scale have also been presented. These are mainly modified versions of the Hodgkin–Huxley model and are capable of handling different types of cell and ions currents. Nobel [37] introduced a model that describes the excitation in Purkinje cells; the Beeler–Reuter model [38] introduces the action potential of ventricular myocardium cells, where four currents are included, and the Lou–Rudy model [39], which is a modified version of the Beeler–Reuter model, introduces information about extracellular and intercellular domains. Multicellular models (tissue scale) have also been developed that describe the excitation propagation of action potential in the whole tissue. They can be used in a single cell scale as well. The most used model was introduced by FitzHugh and Nagumo (FHN) [40], and represents the excitation part of the monodomain RDE with two variables representing the depolarization and the repolarization of the cell membrane. Some analysis that measures the stability of excitable tissues in 2D using FHN and single or multiple noise sources is also presented [41,42]. The FHN model is simplified and presented in different forms [43,44] but was updated by Aliev and Panfilov [45,46], where they modified the normalized form of the FHN model to include the effect of action potential duration. The Aliev–Panfilov model contains two variables as in the following equations: the fast variable u that represents the fast action of cell depolarization and the slow variable v that represents the slow action of cell repolarization.

$$f = ku(u-a)(1-u) - uv \tag{5}$$

$$\frac{\partial v}{\partial t} = \varepsilon(u,v)(-v - ku(u-a-1)) \tag{6}$$

$$\varepsilon(u,v) = \varepsilon_0 + \frac{\mu_1 v}{u+\mu_2}, \tag{7}$$

where for the heart tissues, $k = 8$, $a = 0.15$, $\varepsilon_0 = 0.002$, $\mu_1 = 0.2$, and $\mu_2 = 0.3$.

2.5. Finite element modeling of monodomain RDE

Substituting in Eq. (4) with Eqs. (5) and (6) and discretizing it using Taylor expansion series yields

$$u^{t+1} = u^t + dt[\nabla.(D\nabla u^t)] + dt[ku^t(u^t-a)(1-u^t) - u^t v^t] + dt[g(I_{app})] \tag{8}$$

$$v^{t+1} = v^t + dt[\varepsilon(u^t, v^t)(-v^t - ku^t(u^t - a - 1))], \tag{9}$$

where dt is the unit time step and X^{t+1} and X^t represent the next and the current values of the variable, respectively. The initial values of u and v are taken to be equal to zero, such that $0 \leq \quad u \quad \leq 1$ and $0 \leq v \quad \leq 1$. The diffusion term can be written as

$$\nabla.(D\nabla u) = \begin{bmatrix} d_{11}\frac{\partial^2 u}{\partial x^2} + d_{22}\frac{\partial^2 u}{\partial y^2} + d_{33}\frac{\partial^2 u}{\partial z^2} + \\ 2d_{12}\frac{\partial^2 u}{\partial x \partial y} + 2d_{23}\frac{\partial^2 u}{\partial y \partial z} + 2d_{13}\frac{\partial^2 u}{\partial x \partial z} + \\ \frac{\partial u}{\partial x}\left[\frac{\partial d_{11}}{\partial x} + \frac{\partial d_{21}}{\partial y} + \frac{\partial d_{31}}{\partial z}\right] + \\ \frac{\partial u}{\partial y}\left[\frac{\partial d_{12}}{\partial x} + \frac{\partial d_{22}}{\partial y} + \frac{\partial d_{32}}{\partial z}\right] + \\ \frac{\partial u}{\partial z}\left[\frac{\partial d_{13}}{\partial x} + \frac{\partial d_{23}}{\partial y} + \frac{\partial d_{33}}{\partial z}\right] \end{bmatrix} \tag{10}$$

RDE is bounded by some conditions, where for each point $\boldsymbol{x}$:

$$\boldsymbol{x} \in \boldsymbol{B}, \text{where } \mathbf{B} \text{ is the heart's tissue domain} \tag{11}$$

$$\boldsymbol{t} \geq \mathbf{0} \tag{12}$$

$$\boldsymbol{u}(\boldsymbol{x}, \mathbf{0}) = \boldsymbol{u_0}, \quad \boldsymbol{u_0} \text{is the initial value of the normalized transmembrance potential.} \tag{13}$$

$$\boldsymbol{v}(\boldsymbol{x}, \mathbf{0}) = \boldsymbol{v_0}, \quad \boldsymbol{v_0} \text{is the initial value of the slow variable of the repolarization.} \tag{14}$$

$$\boldsymbol{n}\boldsymbol{\nabla}\boldsymbol{u} = \mathbf{0} \text{ on } \boldsymbol{\partial B} \tag{15}$$

2.6. Modified version of monodomain RDE

The diffusion part of the monodomain RDE is usually used for myocardium tissues only, which makes it work with homogeneous–anisotropic material. However, by including Purkinje tissues beside myocardium tissues, the material becomes inhomogeneous–anisotropic, which requires slight modifications in the D term. It was reported that the longitudinal and the traverse conductivities of myocardium take the values σ_{il} =34.4 mS/mm, and σ_{it} =5.96 mS/mm [47]; however for Purkinje fibers σ_{il} = 95 mS/mm and σ_{it} = 12.15 mS/mm [48]. To maintain normalization of the RDE equation, it is necessary to normalize the conductivity tensor of whole heart tissues referring to Purkinje fibers longitudinal conductivity instead of myocardium; then Eq. (3) becomes

$$D' = e \begin{bmatrix} \sigma_{il}/\sigma_{il\_Purk} & 0 & 0 \\ 0 & \sigma_{it}/\sigma_{il\_Purk} & 0 \\ 0 & 0 & \sigma_{it}/\sigma_{il\_Purk} \end{bmatrix} e^T, \tag{16}$$

where σ_{il_Purk} is the longitudinal conductance of the Purkinje fibers.

According to physical measurements, the speed of action potential propagation in myocardium fibers ranges from 0.3 to 0.5 m/s, while it ranges from 2.5 to 4 m/s in Purkinje fibers [49]. This means the Purkinje

fibers conduct action potential almost 8 times faster than the myocardium fiber. To achieve this, dt in Eq. (9) should be changed to dt', where

$$dt' = \begin{cases} dt & Myocardium \\ 8dt & Purkinje \end{cases} \tag{17}$$

Then, finally, Eq. (8) can be written as

$$u^{t+1} = u^t + dt'[\nabla.(D'\nabla u^t)] + dt'[ku^t(u^t - a)(1 - u^t) - u^t v^t] + dt'[g(I_{app})] \tag{18}$$

Unlike other studies, with the proposed model of the conduction system and the modified RDE equation (Eq. (18)), it is possible to model realistic heart activation very easily without worrying about synchronization of activation or the correct locations of activation sites, which are assigned manually as in previous studies. It is only required to assign the value of the external applied input term $dt[g(I_{app})]$ of Eq. (18) to 1 in regions of the AV node and zero elsewhere, and activation of the heart will be generated automatically in both conduction system and myocardium.

3. Results

The implementation of the solution was accomplished using the C/C++ programming language and MATLAB. The OpenGL library was used to visualize the excitation propagation of the heart. It took about 180 h (i5 processor, 3.2 GHz, 8 GB RAM) for generating the propagation isochrones. The excitation propagation of normal activation was implemented according to the modified RDE and the conduction system, which has been extracted using the DV method as shown in Figure 3, where the top-left slice is close to the base of the ventricles, and the bottom-right slice is close to the heart's apex as well as some intermediate slices. The dark red region in the third slice at the top row is close to the AV node where the excitation has been initialized. Zones of the conduction system far away from the start activation zone have less red intensity, as some time is required until the activation reaches them; however, they were excited much faster than myocardium (which is the real case).

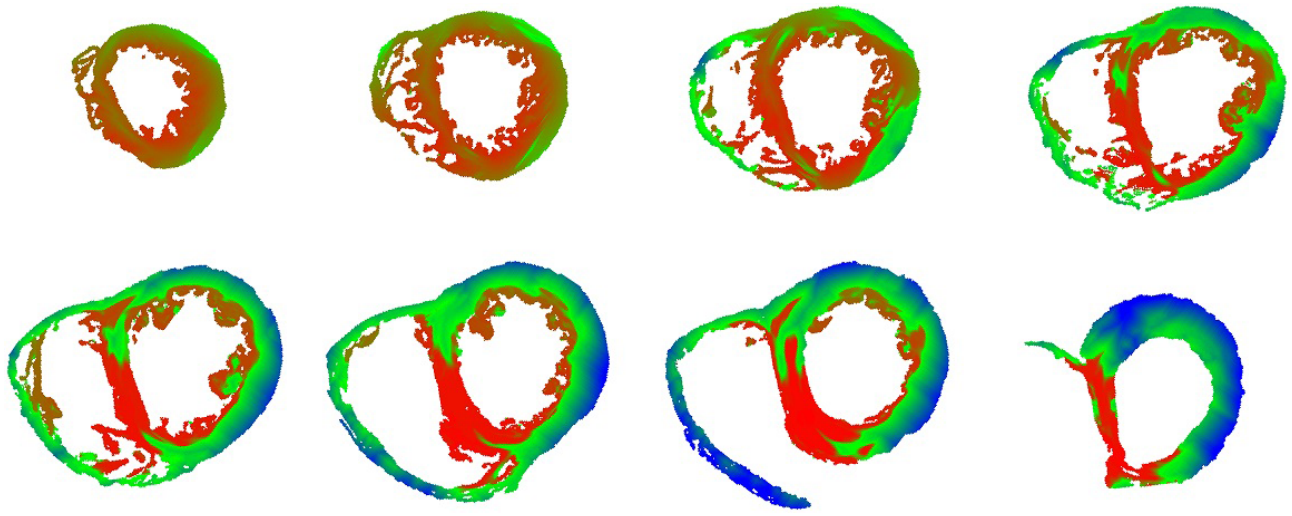

Figure 3. Sample of excitation isochrones of normal heart activation.

4. Discussion and conclusion

Modeling the excitation propagation inside the heart has been accomplished based on a conduction system that is extracted from DV maps and a modified version of RDE. The Aliev–Panfilov method is used to model the reaction part of the equation and inhomogeneous–anisotropic diffusion is used to model the diffusion part of the equation. The time step of Purkinje tissues has been modified to become 8 times the myocardium time step to achieve real measurements. For testing the time step variation effect, two 3D experimental samples of tissues ($10 \times 10 \times 100$ vortexes) have been used (Figure 4). One is totally myocardium and the other is myocardium with a Purkinje fiber core, and both have horizontal fiber direction. After running the modified RDE on both samples with the same pacing site and the same number of time steps, excitation propagates 8 times faster in Purkinje tissue than in myocardium tissue.

Figure 4. (a) Myocardium tissue sample excitation propagation simultaneous with (b) excitation propagation in Purkinje tissue sample.

Employing the proposed conduction system and the modified RDE on the heart model shows (somewhat) realistic heart activation (Figure 5). The produced ventricular excitation propagation isochrones are similar to the measurements reported by Durrer et al. [9]. The remarkable nature of this propagation is that the activation starts in the endocardium wall and propagates towards the epicardium wall through the myocardium. The anterior parts of the free walls are activated later than the posterior ones. The RV completes its depolarization later than the LV. However, these isochrones may not be identical, as the conduction systems of different human hearts do not have identical structures [8].

Abbreviations

DTI Diffusion tensor imaging
RA Right atrium
LA Left atrium
RV Right ventricle
LV Left ventricle
IV septum Interventricular septum
AV node Atrioventricle node
SA node Sinoatrial node
SCD Sudden cardiac death
DTI Diffusion tensor imaging
MD Mean diffusivity
DV Diffusion volume
ECG Electrocardiograph
MCG Magnetocardiograph
RDE Reaction diffusion equation
FHN FitzHugh and Nagumo

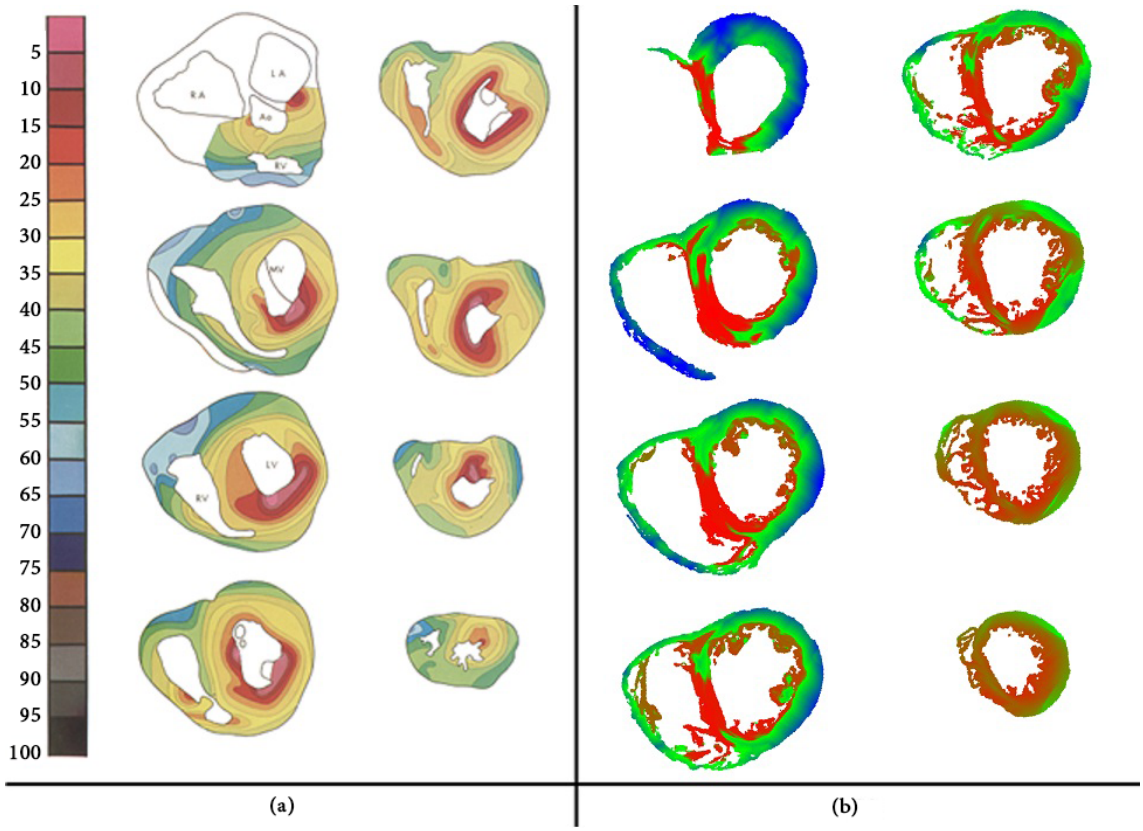

Figure 5. Activation isochrones of the normal activation of ventricles (a) from Durrer et al.'s measurements [9] (b) using the proposed conduction system and the modified RDE.

Acknowledgments

Dr Patrick A Helm and Dr Raimond L Winslow at the Center for Cardiovascular Bioinformatics and Modeling of Johns Hopkins University and Dr Elliot McVeigh at the National Institute of Health for provision of DT-MRI data.

References

[1] Jordan PN, Christini DJ. Therapies for ventricular cardiac arrhythmias. Crit Rev Biomed Eng 2005; 33: 557-604.

[2] Tortora GJ, Derrickson B. Principles of Anatomy and Physiology. 11th ed. Oxford, UK: John Wiley & Sons, Inc., 2006.

[3] Standring S. Gray's Anatomy. 39th ed. New York, NY, USA: Elsevier Churchill Livingstone, 2005.

[4] Brooker C. Human Structure and Function. 2nd ed. London, UK: Mosby Int. Ltd., 1998.

[5] Kessel RG. Basic Medical Histology: The Biology of Cells, Tissues, and Organs. Oxford, UK: Oxford University Press, Inc., 1998.

[6] Widmaier EP, Raff H, Strang KT. Vander's Human Physiology: The Mechanisms of Body Function. 10th ed. Boston, MA, USA: McGraw-Hill, 2006.

[7] Tawara S. The Conduction System of the Mammalian Heart. English ed. London, UK: Imperial College Press, 2000.

[8] Massing GK, James TN. Anatomical configuration of the His bundle and bundle branches in the human heart. Circulation 1976; 53: 609-621.

[9] Durrer D, Van Dam RTH, Freud GE, Janse MJ, Meijler FL, Arzbaecher RC. Total excitation of the isolated human heart. Circulation 1970; 41: 899-912.

[10] Ohyu S, Okamoto Y, Kuriki S. Use of the ventricular propagated excitation model in the magnetocardiographic inverse problem for reconstruction of electrophysiological properties. IEEE T Bio-Med Eng 2002; 49: 509-518.

[11] Sermesant M, Delingette H, Ayache N. An electromechanical model of the heart for image analysis and simulation. IEEE T Med Imaging 2006; 25: 612-625.

[12] Pollard AE, Barr RC. The construction of an anatomically based model of the human ventricular conduction system. IEEE T Bio-Med Eng 1990; 37: 1173-1185.

[13] Ohyu S, Okamoto Y, Kuriki S. Use of the ventricular propagated excitation model in the magnetocardiographic inverse problem for reconstruction of electrophysiological properties. IEEE T Bio-Med Eng 2002; 49: 509-518.

[14] Farina DS, Skipa O, Kaltwasser C, Dossel O, Bauer WR. Personalized model of cardiac electrophysiology of a patient. International Journal of Bioelectromagnetism 2005; 7: 303-306.

[15] Berenfeld O, Jalife J. Purkinje-muscle reentry as a mechanism of polymorphic ventricular, arrhythmias in a 3-dimensional model of the ventricles. Circ Res 1998; 82: 1063-1077.

[16] Simeliusa K, Nenonena J, Horacekb M. Modeling cardiac ventricular activation. International Journal of Bioelectromagnetism 2001; 3: 51-58.

[17] Lorange M, Gulrajani RM. A computer heart model incorporating anisotropic propagation. J Electrocardiol 1993; 26: 245-261.

[18] Smaill BH, LeGrice IJ, Hooks DA, Pullan AJ, Caldwell BJ, Hunter PJ. Cardiac structure and electrical activation: Models and measurement. Proc Aust Physiol Pharmacol Soc 2004; 34: 141-149.

[19] Knisley SB, Trayanova N, Aguel F. Roles of electric field and fibre structure in cardiac electric stimulation. Biophys J 1999; 77: 1404-1417.

[20] Berger T, Fischer G, Pfeifer B, Modre R, Hanser F, Trieb T, Roithinger FX, Stuehlinger M, Pachinger O, Tilg B et al. Single-beat noninvasive imaging of cardiac electrophysiology of ventricular pre-excitation. J Am Coll Cardiol 2006; 48: 2045-2052.

[21] El-Aff I. Extraction of human heart conduction network from diffusion tensor MRI. In: IASTED BioMed 2010; 17–19 February 2010; Innsbruck, Austria: pp. 680-051.

[22] Sommer JR, Johnson EA. Cardiac muscle: A comparative study of Purkinje fibres and ventricular fibres. J Cell Biol 1968; 36: 497-526.

[23] Hurst JW, Logue RB, Schlant RC, Wenger NK. The Heart. 3rd ed. New York, NY, USA: McGraw-Hill, 1974.

[24] Eliska O. Purkinje fibers of the heart conduction system: The history and present relevance of the Purkinje discoveries. Casopis Lekaru Ceskych 2006; 145: 329-335.

[25] Margulis AR. Open Field Magnetic Resonance Imaging: Equipment, Diagnosis and Interventional Procedures. 1st ed. New York, NY, USA: Springer-Verlag Telos, 2000.

[26] Stark DD, Bradley WG. Magnetic Resonance Imaging. 3rd ed. Maryland Heights, MO, USA: C.V. Mosby, 1999.

[27] Lufkin RB. The MRI Manual. 2nd ed. Maryland Heights, MO, USA: C.V. Mosby, 1998.

[28] Bushong SC. Magnetic Resonance Imaging: Physical and Biological Principles. 3rd ed. Maryland Heights, MO, USA: Mosby, 2003.

[29] Elaff I, El-Kemany A, Kholif M. Universal and stable medical image generation for tissue segmentation (The unistable method). Turk J Electr Eng & Comp Sci 2017; 25: 1070-1081.

[30] Geselowitz DB. On bioelectric potentials in an inhomogeneous volume conductor. Biophys J 1967; 7: 1-11.

[31] Malmivuo J, Plonsey R. Bioelectromagnetism: Principles and Applications of Bioelectric and Biomagnetic Fields. 1st ed. Oxford, UK: Oxford University Press, 1995.

[32] Potse M, Dube B, Vinet A, Cardinal R. A comparison of monodomain and bidomain propagation models for the human heart. IEEE T Bio-Med Eng 2006; 53: 2425-2435.

[33] Wang LW, Zhang HY, Shi PC. Simultaneous recovery of three-dimensional myocardial conductivity and electrophysiological dynamics: a nonlinear system approach. Comput Cardiol 2006; 33: 45-48.

[34] Sermesant M, Coudiere Y, Delingette H, Ayache N, Sainte-Marie J, Chapelle D, Clement F, Sorine M. Progress towards model-based estimation of the cardiac electromechanical activity from ECG signals and 4D images. ESAIM Proc 2002; 12: 153-162.

[35] Seger M, Modre R, Pfeifer B, Hintermuller C, Tilg B. Non-invasive imaging of atrial flutter. Comput Cardiol 2006; 33: 601-604.

[36] Hodgkin AL, Huxley AF. A quantitative description of membrane current and its application to conduction and excitation in nerve. J Physiol 1952; 117: 500-544.

[37] Noble D. A modification of the Hodgkin–Huxley equations applicable to Purkinje fibre action and pacemaker potentials. J Physiol 1962; 160: 317-352.

[38] Beeler GW, Reuter H. Reconstruction of the action potential of ventricular myocardial fibers. J Physiol 1977; 268: 177-210.

[39] Luo CH, Rudy Y. A model of the ventricular cardiac action potential. Depolarization, repolarization, and their interaction. Circ Res 1991; 68: 1501-1526.

[40] FitzHugh R. Impulses and physiological states in theoretical models of nerve membrane. Biophys J 1961; 1: 445-466.

[41] Franovic I, Todorovic K, Perc M, Vasovic N, Buric N. Activation process in excitable systems with multiple noise sources: One and two interacting units. Phys Rev 2015; E92: 062911.

[42] Franovic I, Perc M, Todorovic K, Kostic S, Buric N. Activation process in excitable systems with multiple noise sources: large number of units. Phys Rev 2015; E92: 062912.

[43] Panfilov AV, Hogeweg P. Spiral breakup in a modified FitzHugh–Nagumo model. Phys Lett A 1993; 176: 295-299.

[44] Winfree AT. Varieties of spiral wave behavior: an experimentalist's approach to the theory of excitable media. Chaos 1991; 1: 303-334.

[45] Aliev RR, Panfilov AV. A simple two-variable model of cardiac excitation. Chaos Soliton Fract 1996; 7: 293-301.

[46] Osman Gania M, Ogawa T. Stability of periodic traveling waves in the Aliev–Panfilov reaction–diffusion system. Commun Nonlinear Sci 2016; 33: 30-42.

[47] Roberts DE, Hersh LT, Scher AM. Influence of cardiac fiber orientation on wavefront voltage, conduction velocity, and tissue resistivity in the dog. Circ Res 1979; 44; 701-712.

[48] Weidmann S. The electrical constants of Purkinje fibers. J Physiol 1952; 118: 348-360.

[49] Guyton AC. Human Physiology and Mechanisms of Diseases. 5th ed. Philadelphia, PA, USA: Saunders, 1992.